Computer Methods and Programs in Biomedicine 141 (2017) 3–9

Contents lists available at ScienceDirect

Computer Methods and Programs in Biomedicine

journal homepage: www.elsevier.com/locate/cmpb

An improved arteriovenous classification method for the early diagnostics of various diseases in retinal image

Xiayu Xu[a,b], Wenxiang Ding[a,b], Michael D. Abràmoff[c], Ruofan Cao[a,b,*]

[a] The Key Laboratory of Biomedical Information Engineering, Ministry of Education, School of Life Science and Technology, Xi'an Jiaotong University, Xi'an 710049, P.R. China

[b] Bioinspired Engineering and Biomechanics Center (BEBC), Xi'an Jiaotong University, Xi'an 710049, P.R. China

[c] Department of Ophthalmology and Visual Sciences, University of Iowa, Iowa City, IA 52242, USA

ARTICLE INFO

Article history:
Received 26 August 2016
Revised 6 January 2017
Accepted 16 January 2017

Keywords:
Retinal image
Arteriovenous classification
Image analysis
Computer-aided diagnostics

ABSTRACT

(Background and objectives): Retinal artery and vein classification is an important task for the automatic computer-aided diagnosis of various eye diseases and systemic diseases. This paper presents an improved supervised artery and vein classification method in retinal image.

(Methods): Intra-image regularization and inter-subject normalization is applied to reduce the differences in feature space. Novel features, including first-order and second-order texture features, are utilized to capture the discriminating characteristics of arteries and veins.

(Results): The proposed method was tested on the DRIVE dataset and achieved an overall accuracy of 0.923.

(Conclusion): This retinal artery and vein classification algorithm serves as a potentially important tool for the early diagnosis of various diseases, including diabetic retinopathy and cardiovascular diseases.

1. Introduction

The retinal vasculature provides lots of information about various ophthalmic and systemic diseases, including diabetes mellitus and cardiovascular diseases. However, these diseases may affect arteries and veins differentially [1]. For instance, retinal veins are abnormally dilated in patients with diabetes mellitus and ipsilateral severe extracranial carotid diseases, while arteries are narrowed in high blood pressure [2,3]. Besides, these vascular changes often precede the onset of other signs and symptoms associated with these diseases, which makes the analysis of retinal vessels attractive as a biomarker for the early diagnosis and treatment. Therefore, it is of great interest to develop automated tools for retinal artery and vein classification.

The retinal artery and vein classification methods reported in literature can be divided into tree-based methods and feature-based methods. The former focuses on segmenting retinal vessels into individual biological vessel trees, which can be further classified into artery trees and venous trees. Rothaus et al. reported a semiautomatic approach using a rule-based method that can propagate vessel labels through the vascular graph, in which the labels were manually labeled by user as arteries or veins [4]. Hu et al. proposed a graph-based, meta-heuristic algorithm to separate vessel trees, which was evaluated on 48 fundus images with a false positive rate of 11.03% [5]. A recent work by Estrada et al. incorporated a graph-theoretic framework with a likelihood model, which needs iterative exploration of possible solutions to achieve optimized result. This method achieved a high accuracy of 91.78% from four different datasets [6]. Drawbacks of tree-based methods include the requirement for manual initial labels in some of the methods and the risk that a single mislabel along propagation may lead to mislabel of entire vessel tree, which is almost inevitable as the vessel tree goes to peripheral regions where low contrast is provided. Besides, complicated graph-based method usually asks for high computational cost and long running time. The second strategy is feature-based methods, which take advantage of the fact that retinal arteries and veins in standard retinal fundus imaging show a number of colorimetric and geometric differences [7]. Specifically, arteries contain oxygenated hemoglobin, which has higher reflectance than deoxygenated hemoglobin in specific wavelengths, and are thus brighter than veins. Besides, the central light reflex (CLR) phenomenon, a specular reflection, is more frequently seen in retinal arteries. Various methods have been developed for retinal artery and vein classification based on a single or a combination of these features. For instance, Niemeijer et al. reported a supervised classification method using a *k*-nearest neighbor (*k*NN)

* Corresponding author.
E-mail addresses: xiayuxu@xjtu.edu.cn (X. Xu), ruofanc@mail.xjtu.edu.cn (R. Cao).

http://dx.doi.org/10.1016/j.cmpb.2017.01.007
0169-2607/

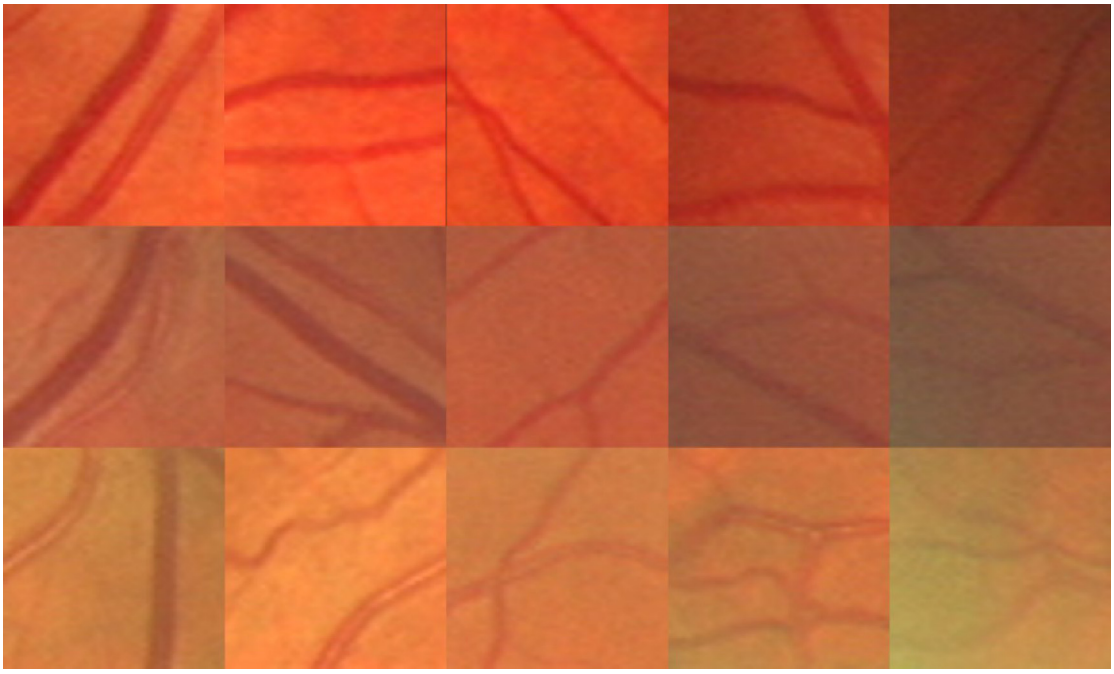

Fig. 1. Examples of intra-image and inter-subject differences. From left to right: inset view of retinal blood vessels from central region to peripheral region of the same image. From top to bottom: inset view of retinal blood vessels from different subjects.

classifier, in which HSV color features and Gaussian derivatives were used as discriminating features and an area under the receiver operator characteristic (ROC) curve of 0.88 was reported [8]. Saez et al. reported an unsupervised method based on a clustering algorithm to distinguish arteries and veins using RGB/HSL color and gray level as the discriminating features, which gave a sensitivity of 0.78 for arteries and 0.87 for veins [9]. However, several important characteristics of retinal images are neglected in these methods. First, retinal image suffers from an inherited inhomogeneous brightness caused by uneven illumination during image acquisition, resulting in very different appearances of blood vessels near the center of the image and at peripheral regions, which can be even larger than the differences between arteries and veins. Moreover, the inter-subject background varies a lot due to biological characteristics (as shown in Fig. 1), showing different distributions in feature space. To address these, Vazquez et al. proposed a retinex image enhancement method to adjust the uneven illumination inside an image, which improved the classification result to an accuracy rate around 90% [10]. Relan et al. reported an unsupervised method based on a Gaussian mixture model and an expectation-maximization clustering on illumination-corrected retinal images, which gave an accuracy of 0.87 for veins and 0.85 for arteries [11]. Although improvement has been achieved in these methods through considering intra-image differences, inter-subject differences were not considered. Besides, relatively simple features, such as different RGB and HSV color spaces, have been considered as discriminating features in most reported methods. We propose that more complicated features may be more efficient in distinguishing retinal arteries and veins. For example, the exact vessel width can reflect the major geometric difference between arteries and veins while the image texture is able to show not only color features but also geometric features, including the sharpness of vessel boundary and the coarseness inside a blood vessel [12]. Thus, we introduce several novel features in this work trying to improve the efficiency of classification.

In this paper, we propose to improve the retinal artery and vein classification in two ways. First of all, background adjustment is applied to decrease the intra-image differences, *i.e.*, the differences between central region and peripheral regions. Moreover, an inter-subject normalization is introduced to minimize the color differences between subjects. Second, we introduce several novel features, including the exact vessel width and the first and second order texture features.

2. Materials

The vessel classification method was evaluated on a popular publicly available database, the DRIVE (Digital Retinal Image for Vessel Extraction) database, which includes a set of forty color fundus photographs obtained from a diabetic retinopathy screening program [13]. In this dataset, seven out of forty images contain pathologies such as exudates, hemorrhages and pigment epithelium changes. The images, with a size of 768×584 pixels, were acquired using a Canon CR5 non-mydriatic 3-CCD camera with a field-of-view (FOV) of 45°. DRIVE database is divided into two sets, the training set and the test set, each containing twenty images. The test set, manually segmented by two observers and the first observer is accepted as ground truth, was included in this study. The vessels from the test set was manually labeled as artery, vein, or overlapping by a trained ophthalmologist.

3. Methods

The flowchart of our approach is given in Fig. 2. Initially, the intra-image regularization and inter-subject normalization is applied and the blood vessels are extracted based on image salient features. During training phase, multiple image features are extracted from each vessel centerline pixel and a likelihood model is established. During test phase, the same features are extracted for each centerline pixel and classified using a kNN classifier. For each test pixel, the output value of the classifier is the average of the labels of the k nearest neighbors in feature space, resulting in a gray-scale probability image. In this image, lower gray level indicates a higher probability of being a vein while higher gray level indicates a higher probability of being an artery. At last, a voting

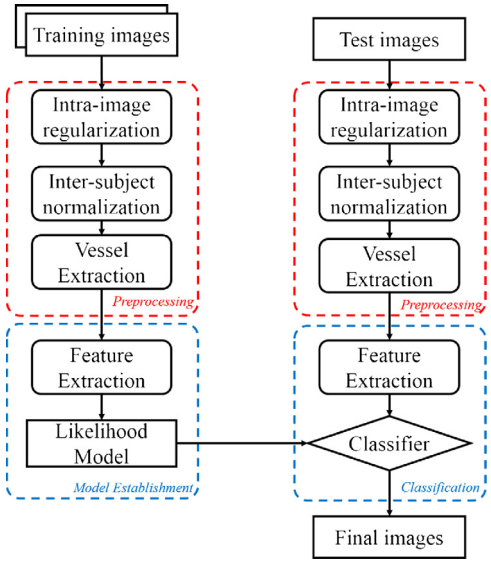

Fig. 2. Flowchart of proposed algorithm.

procedure is applied to achieve a consistent classification for each vessel segment.

3.1. Preprocessing

Fundus image suffers from inhomogeneous background color due to uneven illumination on the curved surface of retina during imaging. Hence, before the inter-subject normalization, a background regularization is performed by applying a high-pass filter on the image. To do this, a Gaussian filter with large kernel is convolved with the original image (Fig. 3a) to remove the high frequency information, leaving only the slowly changing background, which is then subtracted from the original image (Eq. 1).

$$R(x,y) = I(x,y) - \varphi(x,y) * I(x,y), \tag{1}$$

$$\varphi(x,y) = \frac{1}{\sqrt{2\pi\sigma^2}} e^{-\frac{x^2+y^2}{2\sigma^2}}, \tag{2}$$

where φ denotes a Gaussian filter with a σ of 5, *I(x,y)* denotes the original image, and *R(x,y)* denotes the background-removed residual image (Fig. 3b). After the intra-image background regularization, an inter-subject normalization is performed to reduce the difference between images obtained from different subjects. This is especially important in supervised classification methods as it can reduce the differences between training and test data. To perform the normalization, the histograms of the red, green, and blue channels are calculated and the median values are found individually. Then a brightness curve transform is performed in each channel to move the median value to a unified center (Eq. 3).

$$g(x,y) = \max(\min(I(x,y) - median(H) + c, 255), 0) \tag{3}$$

where H denotes the histogram of image I(x,y), c denotes the unified center (128 in this study), and g denotes the image after brightness curve transform (Fig. 3c).

The retinal vessel is extracted from the retinal image using a saliency-based vessel segmentation method. Various salient features, including spectral residual, Gabor-based orientation feature, morphological feature, and self-information, are extracted. The final binary blood vessel image is created by a linear combination of all normalized saliency features (Fig. 3d). Detailed method description and validation can be found in Xu et al. [14]. This method gave an accuracy of 93.3% for the DRIVE database in the validation study. Vessel skeleton is generated from the binary vessel image through sequential thinning, followed by the removal of branching and crossing points, leaving individual vessel segments for feature extraction.

3.2. Feature extraction

For each vessel centerline pixel, the normal direction is calculated. Three adjacent centerline pixels from both sides are included in a principle component analysis. The second principal component corresponds to the normal direction of the target centerline pixel. For an end point without enough neighboring centerline pixels, the normal direction follows the nearest valid centerline pixel, *i.e.*, a centerline pixel with a normal direction. Two types of data are used for feature calculation, namely single profile and image patch (Fig. 4). Single profile *p(x)* is a one-dimensional function sampled

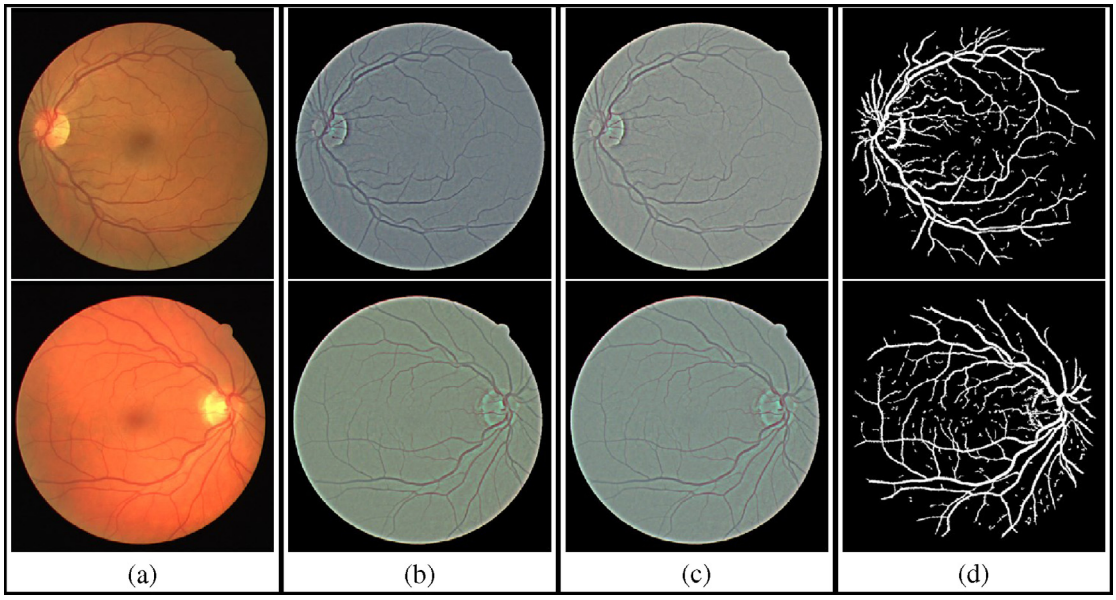

Fig. 3. Preprocessing of retinal images. (a) Original retinal image. (b) After intra-image background regularization. (c) After inter-subject normalization. (d) Vessel segmentation result.

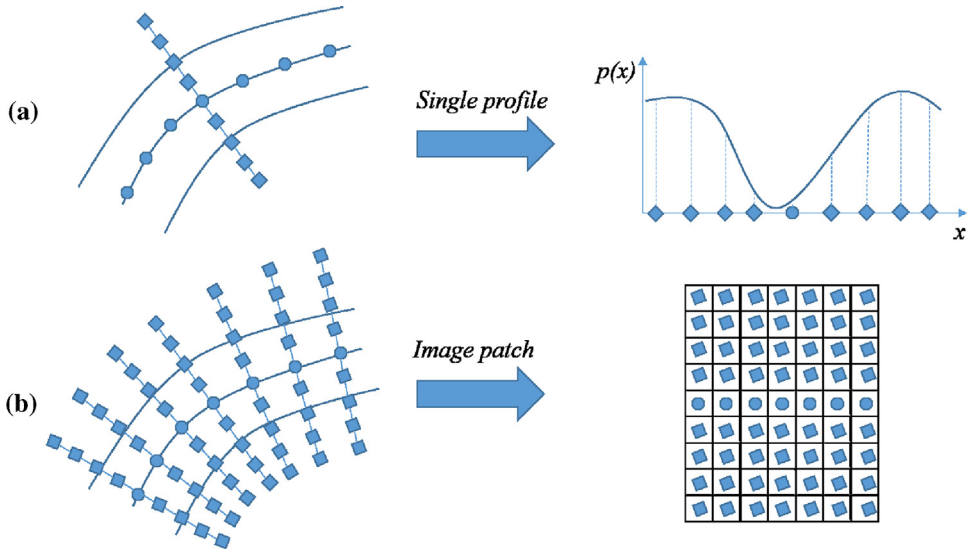

Fig. 4. Illustration of the two types of data used in feature calculation. (a) Single profile $p(x)$ is a one-dimensional function sampled along the normal direction of the target centerline, used in the extraction of vessel width and central light reflex (CLR) features. (b) Image patch is a two-dimensional image sampled along the normal direction of the target centerline and its adjacent neighboring centerlines, covering a neighboring region for feature extraction.

Table 1
The complete set of features extracted for artery and vein classification.

Category	Name	Description	Index
Profile	Vessel Width	The precise width of a vessel profile in pixel.	1
	CLR Std	The standard deviation of a vessel profile, characterizing the central light reflex property.	2
	CLR Skewness	The skewness of a vessel profile, characterizing the central light reflex property.	3
	CLR Kurtosis	The kurtosis of a vessel profile, characterizing the central light reflex property.	4
Color	CIExyY x	The average x value of a vessel segment in CIExyY color space.	5
	CIExyY y	The average y value of a vessel segment in CIExyY color space.	6
	CIExyY Y	The average Y value of a vessel segment in CIExyY color space.	7
Texture-FOS	Mean	The mean of the first order statistic texture features of a vessel segment.	8
	Std	The standard deviation of the first order statistic texture feature of a vessel segment.	9
	Skewness	The skewness of the first order statistic texture feature of a vessel segment.	10
	Kurtosis	The kurtosis of the first order statistic texture feature of a vessel segment.	11
Texture-GLCM	Energy	The energy of the GLCM texture feature of a vessel segment. Degrees 0 and 90 were used.	12–13
	Entropy	The entropy of the GLCM texture feature of a vessel segment. Degrees 0 and 90 were used.	14–15
	Contrast	The contrast of the GLCM texture feature of a vessel segment. Degrees 0 and 90 were used.	16–17
	Homogeneity	The homogeneity of the GLCM texture feature of a vessel segment. Degrees 0 and 90 were used.	18–19
	Correlation	The correlation of the GLCM texture feature of a vessel segment. Degrees 0 and 90 were used.	20–21

along the normal direction of the target centerline, used in the extraction of vessel width and CLR features. Image patch is a two-dimensional matrix sampled along the normal direction of the target centerline and its adjacent neighboring centerlines, covering a neighboring region for feature extraction. The size of the image patch was empirically set to cover the width of the widest vessel in the image (8 pixels $\times$ 8 pixels for the DRIVE dataset). All features are normalized to [0, 1] and a list of all 21 features is given in Table 1.

(1) *Single profile features:* the first set of features is extracted from the single cross-sectional profile $p(x)$, including vessel width and CLR features. The precise vessel width of a single cross-sectional profile is calculated using graph-based method [15]. This method is able to find the left and right boundaries simultaneously by modeling the two-boundary problem into a single three-dimensional optimal surface problem, after which the vessel width is calculated as the distance between the left and right boundaries. As mentioned above, CLR is more frequently seen in arteries. We use the standard deviation, skewness, and kurtosis to characterize the shape of the single profile (Table 2).
(2) *Color features:* The color features are extracted from an image patch centered at the target centerline pixel. The CIExyY

Table 2
The definitions of first order and second order texture features.

Category	Name	Definition
First order statistics	Mean	$\mu = \sum_{i=1}^{N} x_i p_i$
	Standard deviation	$\sigma = \sqrt{\frac{1}{N}\sum_{i=1}^{N}(x_i-\mu)^2}$
	Skewness	$\gamma_1 = \frac{E[(X-\mu)^3]}{(E[(X-\mu)^2])^{3/2}}$
	Kurtosis	$\gamma_2 = \frac{E[(X-\mu)^4]}{(E[(X-\mu)^2])^2}$
GLCM Image Texture	Energy	$Energy = \sum_{i,j=0}^{N-1} (P_{ij})^2$
	Entropy	$Entropy = \sum_{i,j=0}^{N-1} -\ln(P_{ij})P_{ij}$
	Contrast	$Contrast = \sum_{i,j=0}^{N-1} P_{ij}(i-j)^2$
	Homogeneity	$Homogeneity = \sum_{i,j=0}^{N-1} \frac{P_{ij}}{1+(i-j)^2}$
	Correlation	$Correlation = \sum_{i,j=0}^{N-1} P_{ij} \frac{(i-\mu)(j-\mu)}{\sigma^2}$

P_{ij}: Element i, j of the normalized symmetrical GLCM.
N: Number of gray levels in the image.

color space is used to characterize the color properties of the vessel, in which the chromaticity of a color was specified by two parameters x and y and the brightness is specified by a third parameter Y. The average values of x, y, and Y within the image patch are used.

(3) *Texture features:* Both first-order statistics (FOS) and second-order statistics such as gray-level co-occurrence matrix (GLCM) are analyzed for the image patch centered at the target centerline pixel. FOS texture features are related to the gray level distribution (*i.e.*, histogram) of an image path and ignore inter-pixel correlations. In contrast, second-order statistics consider the spatial relationship of pixels in an image patch, making it angle dependent. GLCM is a common second-order texture analysis, which describes the texture of an image by giving the frequency of the pairs of pixels that are with specific values and in a specific spatial relationship. Both degree 0 and degree 90 are calculated in this study. Specific parameters extracted from GLCM analysis include energy, entropy, contrast, homogeneity, and correlation. The details of texture feature calculation is given in Table 2. Texture features are extracted from the green channel of the image, which usually shows the best contrast [16].

3.3. Training phase

A supervised classification method is used, in which a classifier is established during the training phase and then used to classify unknown test images in the future. For each training image, the vessel is first segmented and the vessel centerline pixels are generated through a sequential thinning method. Then the vessel branching points and crossing points are removed, resulting in individual vessel segments. For each vessel centerline pixel, all features mentioned above are extracted. A leave-one-out cross validation method is used because of the small sample size.

3.4. Test phase

During the test phase, for each previously unseen image, the same preprocessing is applied, including intra-image regularization, inter-subject normalization, and vessel centerline extraction. Similarly, branching points and crossing points are excluded from further analysis. For each vessel centerline pixel, the same set of features is extracted as input to a *k*NN classifier with a Euclidean distance metric. Initially, three classifiers, including kNN, neuron network, and decision tree, were compared using Weka 3 [17]. The kNN classifier outperformed the other two classifiers and was selected in this study. The output is a soft label ranging from 0 to 1, in which a higher soft label indicates a higher probability of being arteries and vice versa for veins. After obtaining the classification result for each vessel centerline, a voting procedure is taken inside each vessel and the majority voting is determined as the final classification for the whole vessel segment.

4. Results

To evaluate the result of our method, the true positive rate for arteries and veins were calculated respectively. For each detected vessel centerline pixel, a truth label is obtained from the manually classified ground truth image with 0 denotes vein and 1 denotes artery. The vessel centerline pixels without a truth label will be discarded. TPR_A is defined as the ratio of correctly classified artery centerline pixels to all centerline pixels with a label 'artery' . Similarly, TPR_V is defined as the ratio of correctly classified vein centerline pixels to all centerline pixels with a label 'vein' . Finally, Acc is defined as the ratio of all correctly detected centerline pixels to all centerline pixels with a ground truth label. All centerline pixels with a true label in the truth image are included, resulting in a total number of 73,003 for finally classified centerline pixels. The accuracy is 0.915 for arteries and 0.929 for veins, respectively, while the overall accuracy is 0.923. Table 3 summarizes the TPR_A, TPR_V, and Acc for all images in the DRIVE test set. Fig. 5 shows three sample results from the DRIVE dataset. For each sample, the first column is the original fundus image, the second column is the manual classification of all vessels by an expert, and the last column shows the final classification with proposed method.

Table 3
Results on individual images from the DRIVE test dataset.

Index	TPR_A	TPR_V	Acc
1	0.931	0.920	0.926
2	0.857	0.969	0.920
3	0.908	0.968	0.944
4	0.999	0.863	0.936
5	0.916	0.938	0.927
6	0.945	0.982	0.965
7	0.970	0.968	0.969
8	0.914	0.941	0.930
9	0.966	0.967	0.967
10	0.930	0.954	0.943
11	0.889	0.945	0.918
12	0.874	0.948	0.918
13	0.957	0.936	0.945
14	0.880	0.946	0.916
15	0.968	0.837	0.915
16	0.868	0.959	0.917
17	0.809	0.802	0.805
18	0.994	0.961	0.977
19	0.884	0.853	0.866
20	0.804	0.901	0.861
Overall	**0.915**	**0.929**	**0.923**

The proposed method was implemented in C++ and tested on a 3.40 GHz Intel® Core™ i7-3770 CPU with 8GB of RAM. It took ~40 seconds to build the likelihood model and ~5 seconds to run a test image from the DRIVE dataset.

5. Discussion and conclusion

In this work, we showed an improved supervised retinal artery and vein classification method. Retinal artery and vein classification is a challenging task because of the inhomogeneous brightness caused by uneven illumination and because of the substantial inter-subject background variation such as pigmentation patterns (Fig. 1). We hypothesized that by implementing intra-image and inter-subject normalization, the inhomogeneity in features as induced by color differences could be reduced and that more sophisticated features such as image texture would lead to improved performance distinguishing arteries from veins. Our hypothesis was confirmed by an accuracy of 0.915 for artery and 0.929 for vein, which outperformed previous pixel-based methods without intra-image and inter-subject normalization [8,9].

There are several limitations of our proposed method. Firstly, our approach was developed and tested on a small set of high-resolution retinal images and its performance on low quality retinal images has not yet been assessed. The method can be improved by including nonmydriatic, low quality retinal images obtained at point-of-care settings in the training set. A second limitation is that the proposed pixel-based classification method cannot guarantee the connectivity of the vessel tree, which is a useful prior for further image analysis, such as for the calculation of arteriolar-to-venular ratio and branching angle [10,18–20]. Tree-based methods show great advantage in this aspect [21]. Our future work will focus on the establishment of continuous topological trees based on the achieved artery and vein classification, in

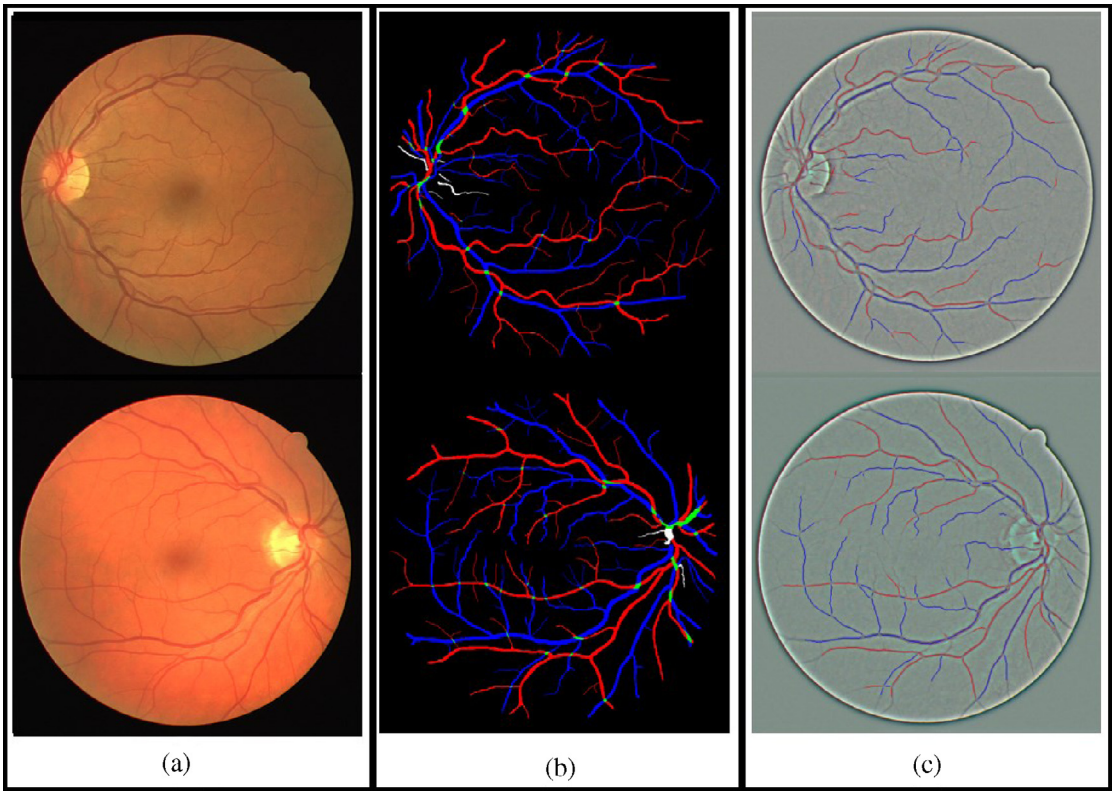

Fig. 5. Sample classification results. (a) Original fundus images. (b) Truth images from human expert. (c) Automatic classification results.

which the proposed method can provide prior information for the establishment of continuous topological trees [22].

Many properties of retinal arteries and veins have been shown to change after the development and during the course of various ocular and systemic diseases, such as diabetic retinopathy and cardiovascular diseases [23–26]. The establishment of an automatic artery and vein classification method, combined with vessel width measurement [15,27], helps to understand the clinical significance of retinal vascular changes in a more efficient way. Another potential usage of the proposed automatic artery and vein classification method is in the establishment of a computer-aided diagnostic/screening tool for resource-limited settings, where professional personnel are not always available [28].

In summary, we proposed an improved method for retinal artery and vein classification by applying intra-image and inter-subject normalizations. Novel features such as first order and second order image texture were implemented to improve the efficiency of classification. This method showed an overall accuracy of 0.923 and high computational performance of ~5 seconds per image. This method holds great potential for computer-aided diagnosis of various diseases.

Acknowledgements

This work was financially supported by the National Natural Science Foundation of China (81401480), China Postdoctoral Science Foundation (2014M552460, 2016T90929), the International Science & Technology Cooperation Program of China (2013DFG02930), and National Instrumentation Program (2013YQ190467). MDA is supported the by the Robert C. Watzke Professorship, and the US Department of Veterans Affairs I01 CX000119, and has patent and patent applications on a competing approach. The remaining authors declare no competing financial interest.

References

[1] T.T. Nguyen, J.J. Wang, T.Y. Wong, Retinal vascular changes in pre-diabetes and prehypertension: new findings and their research and clinical implications, Diabetes Care 30 (10) (2007) 2708–2715.
[2] J. Grauslund, et al., Retinal vessel calibre and micro- and macrovascular complications in type 1 diabetes, Diabetologia 52 (10) (2009) 2213–2217.
[3] D.A. De Silva, et al., Retinal vascular caliber and extracranial carotid disease in patients with acute ischemic stroke: the Multi-Centre Retinal Stroke (MCRS) study, Stroke 40 (12) (2009) 3695–3699.
[4] K. Rothaus, X. Jiang, P. Rhiem, Separation of the retinal vascular graph in arteries and veins based upon structural knowledge, Image Vision Comput. 27 (7) (2009) 864–875.
[5] Q. Hu, M.D. Abràmoff, M.K. Garvin, Automated separation of binary overlapping trees in low-contrast color retinal images, Medical Image Computing and Computer-Assisted Intervention–MICCAI 2013, Springer, 2013.
[6] R. Estrada, et al., Retinal artery-vein classification via topology estimation, Med. Imaging IEEE Trans. 34 (12) (2015) 2518–2534.
[7] M.D. Abràmoff, M.K. Garvin, M. Sonka, Retinal imaging and image analysis, Biomed. Eng. IEEE Rev. 3 (2010) 169–208.
[8] M. Niemeijer, B. van Ginneken, M.D. Abràmoff, Automatic classification of retinal vessels into arteries and veins, SPIE medical imaging, International Society for Optics and Photonics, 2009.
[9] M. Saez, et al., Development of an automated system to classify retinal vessels into arteries and veins, Comput Methods Programs Biomed. 108 (1) (2012) 367–376.
[10] S. Vázquez, et al., Improving retinal artery and vein classification by means of a minimal path approach, Mach. Vision Appl. 24 (5) (2013) 919–930.
[11] D. Relan, et al., Retinal vessel classification: sorting arteries and veins, Engineering in Medicine and Biology Society (EMBC), *2013 35th Annual International Conference of the IEEE*, IEEE, 2013.
[12] C. Sun, et al., Retinal vascular caliber: systemic, environmental, and genetic associations, Surv. Ophthalmol. 54 (1) (2009) 74–95.
[13] M. Niemeijer, et al., Comparative study of retinal vessel segmentation methods on a new publicly available database, Medical Imaging 2004, International Society for Optics and Photonics, 2004.
[14] X. Xu, et al., Smartphone-based accurate analysis of retinal vasculature towards point-of-care diagnostics, Sci. Rep. 6 (2016) 34603.
[15] X. Xu, et al., Vessel boundary delineation on fundus images using graph-based approach, Med. Imaging IEEE Trans. 30 (6) (2011) 1184–1191.
[16] S. Lee, M.D. Abramoff, J.M. Reinhardt, Retinal atlas statistics from color fundus images, SPIE Medical Imaging, International Society for Optics and Photonics, 2010.

[17] M. Hall, et al., The WEKA data mining software: an update, SIGKDD Explor. 11 (1) (2009).
[18] J. Staal, et al., Ridge-based vessel segmentation in color images of the retina, Med. Imaging IEEE Trans. 23 (4) (2004) 501–509.
[19] B. Dashtbozorg, A.M. Mendonça, A. Campilho, An automatic graph-based approach for artery/vein classification in retinal images, Image Process. IEEE Trans. 23 (3) (2014) 1073–1083.
[20] E. Grisan, A. Ruggeri, A divide et impera strategy for automatic classification of retinal vessels into arteries and veins, in: Engineering in Medicine and Biology Society, 2003. Proceedings of the 25th Annual International Conference of the IEEE, IEEE, 2003.
[21] M.E. Martinez-Perez, et al., Retinal vascular tree morphology: a semi-automatic quantification, IEEE Trans. Bio-Med. Eng. 49 (8) (2002) 912–917.
[22] K. Li, et al., Optimal surface segmentation in volumetric images-a graph-theoretic approach, Pattern Anal. Mach. Intell. IEEE Trans. 28 (1) (2006) 119–134.
[23] C.Y. Cheung, et al., The clinical implications of recent studies on the structure and function of the retinal microvasculature in diabetes, Diabetologia 58 (5) (2015) 871–885.
[24] S.J. Fahy, et al., The relationship between retinal arteriolar and venular calibers is genetically mediated, and each is associated with risk of cardiovascular disease, Invest. Ophthalmol. Visual Sci. 52 (2) (2011) 975–981.
[25] S.L. Rogers, et al., Retinal arteriolar caliber predicts incident retinopathy: the Australian Diabetes, Obesity and Lifestyle (AusDiab) study, Diabetes Care 31 (4) (2008) 761–763.
[26] T.T. Nguyen, et al., Relationship of retinal vascular caliber with diabetes and retinopathy: the Multi-Ethnic Study of Atherosclerosis (MESA), Diabetes Care 31 (3) (2008) 544–549.
[27] B. Al-Diri, A. Hunter, D. Steel, An active contour model for segmenting and measuring retinal vessels, Med. Imaging, IEEE Trans. 28 (9) (2009) 1488–1497.
[28] T. Khan, et al., Preventing diabetes blindness: cost effectiveness of a screening programme using digital non-mydriatic fundus photography for diabetic retinopathy in a primary health care setting in South Africa, Diabetes Res. Clin. Pract. 101 (2) (2013) 170–176.